Applied Catalysis B: Environmental 90 (2009) 458–462

Contents lists available at ScienceDirect

Applied Catalysis B: Environmental

journal homepage: www.elsevier.com/locate/apcatb

Fe_3O_4 coupled BiOCl: A highly efficient magnetic photocatalyst

Ling Zhang, Wenzhong Wang *, Lin Zhou, Meng Shang, Songmei Sun

State Key Laboratory of High Performance Ceramics and Superfine Microstructures, Shanghai Institute of Ceramics, Chinese Academy of Sciences, 1295 Dingxi Road, Shanghai 200050, PR China

ARTICLE INFO

Article history:
Received 19 December 2008
Received in revised form 1 April 2009
Accepted 4 April 2009
Available online 11 April 2009

Keywords:
Photocatalyst
Magnetic nanoparticles
BiOCl
Coupled structure

ABSTRACT

The magnetic photocatalyst, Fe_3O_4/BiOCl nanocomposite, was prepared and characterized by X-ray diffraction (XRD), transmission electron microscopy (TEM) and high-resolution TEM (HRTEM), physical property measurement system (PPMS). It was found that Fe_3O_4/BiOCl was an effective photocatalyst to degrade the organic dyes. Compared with the conventional core–shell magnetic photocatalysts, such as Fe_3O_4/TiO_2 system which dramatically lost their intrinsically photocatalytic activity due to the introduction of the magnetic core, the as-synthesized Fe_3O_4/BiOCl reserved as high photocatalytic activity as that of BiOCl. The high catalytic activity possibly involved in a coupled structure and the special interfaces, that is, the probability of combination of the carriers could be reduced in this system. Moreover, the superparamagnetic Fe_3O_4/BiOCl can be not only easily recycled but also fluidized by applying an external magnetic field.

1. Introduction

Magnetically separable photocatalyst have attracted increasing attention because of their scientific and technological importance in the environmental purification, especially in waste water treatment [1–3]. Magnetic supports could overcome the limitation of separation from the liquid phase thus the photocatalyst could be effectively recycled by applying an external magnetic field. Currently the researches on the preparation of magnetic photocatalyst mainly focus on the TiO_2/iron oxide composite system. However, most of these pioneer researches in the development of TiO_2 capped Fe_3O_4 photocatalysts suffered from dramatically decreased photocatalytic activities. It resulted from an unfavorable electronic heterojunction between the core–shell TiO_2/Fe_3O_4 which led to the electron–hole recombination [4,5], lower oxidizing power of the photogenerated holes when they transferred to the Fe_3O_4 phase [6], and optically screen of the TiO_2 phase by the Fe_3O_4 phase [7]. Another try was devoted to the amorphous TiO_2 coated on the Fe_3O_4 core which was protected by a SiO_2 insulation layer to avoid unfavorable heterojunction and photodissolution [8,9]. Unfortunately, subsequent heat-treatment for transforming amorphous TiO_2 into crystalline product would lead to the loss of magnetism because of the oxidation of the magnetic core, or the formation of a mixed iron/titanium oxide [10,11]. Recently, the formation of surface phase junction between two phases has been proved to greatly enhance the photocatalytic activity [12–14]. Hence the construction of the special structure and interface phase junction structure would become a promising method for obtaining magnetic photocatalyst with high photocatalytic efficiency.

It has been demonstrated that bismuth oxychloride (BiOCl) has high photocatalytic activity in degrading organic dye [15–17]. Various solution routes have been applied to synthesize this compound [18–20]. Herein we reported the synthesis of BiOCl flake inlaid with Fe_3O_4 nanoparticles. As a highly efficient magnetic photocatalyst for the photodegradation of organic dye under visible light irradiation, it is found that the Fe_3O_4 coupled BiOCl (Fe_3O_4/BiOCl) nanocomposite not only keeps the high photocatalytic activity of the BiOCl flake, but also could be recycled by applying a magnetic filed after the degradation process.

2. Experimental

2.1. Materials

$FeCl_3{\cdot}6H_2O$, $FeSO_4{\cdot}H_2O$, $Bi(NO_3)_3{\cdot}5H_2O$, Sodium dodecyl-benzenesulfonate (SDBS, 95%), $NH_3{\cdot}H_2O$ (28%), Oleic acid (90%), chloroform(Chemical analysis grade) were purchased from Shanghai Chemical Reagent Company and used as received.

2.2. Experimental procedures

2.2.1. Synthesis of the Fe_3O_4 nanoparticles

$FeCl_3{\cdot}6H_2O$ (24.3 g) and $FeSO_4{\cdot}7H_2O$ (16.7 g) were dissolved in 100 ml de-ionized water under nitrogen gas with vigorous stirring at 80 °C. Then 50 ml of ammonium hydroxide were added rapidly

* Corresponding author. Tel.: +86 21 5241 5295.
E-mail address: wzwang@mail.sic.ac.cn (W. Wang).

0926-3373/$ – see front matter © 2009 Elsevier B.V. All rights reserved.
doi:10.1016/j.apcatb.2009.04.005

into the solution. The color of the solution turned to black immediately. Oleic acid (3.76 g) was added after 30 min. Then the suspension was kept at 80 °C for 1.5 h. The magnetite nanoparticles were washed with de-ionized water until the pH value of the system reached neutral. The as-synthesized sample was dried in vacuum at room temperature.

2.2.2. Synthesis of the Fe_3O_4/BiOCl

In a typical synthesis, $Bi(NO_3)_3$ (2.5 mmol) dissolved in 5 ml of a 4 mol/l HNO_3 aqueous solution, was mixed with 15 ml of chloroform containing 10 mmol SDS and 50 mg Fe_3O_4 nanoparticles under stirring. This mixture was then transferred into a 250 ml glass bottle. 5 ml of $NH_3{\cdot}H_2O$ and 10 ml of de-ionized water was added while the reactants were stirred at a speed of 700 rpm. The mixture was heated at 80 °C for 4 h. The brown precipitate formed was isolated by a magnet, washed for several times with de-ionized water and ethanol, and dried at room temperature for 24 h in a laboratory vacuum oven.

Pure BiOCl flakes were also prepared by the same method except introducing the Fe_3O_4 nanoparticles.

2.3. Characterization and analytical methods

2.3.1. X-ray diffraction pattern

The powder X-ray diffraction (XRD) patterns of the as-synthesized samples were measured on a D/MAX 2250 V diffractometer (Rigaku, Japan) using monochromatized Cu Kα (λ = 0.15418 nm) radiation at a scanning rate of 4° min^{-1} with the 2θ ranging from 10° to 70°. The accelerating voltage and applied current were 40 kV and 100 mA, respectively.

2.3.2. TEM analysis

The morphologies and microstructures of as-prepared samples were examined with transmission electron microscopy (TEM, JEOL JEM-2100F; accelerating voltage: 200 kV). High-resolution transmission electron microscopy analysis used the DigitalMicrograph software (Gatan Inc.).

2.3.3. UV–vis absorption spectroscopy

UV–vis spectra were obtained using a Hitatchi U-3010 spectrophotometer and a 1-cm path length quartz cell. The photocatalytic activity of the Fe_3O_4/BiOCl for the decomposition of rhodamine B (RhB) and methylene blue (MB) was evaluated under irradiation of a 500 W Xe lamp and a 420 nm cutoff filter at the natural pH value. The initial concentration of RhB and MB was 30 and 20 mg/l, respectively, with a catalyst loading of 1 g/l. The adsorption balance between the dye solutions and photocatalysts was gained after the suspensions were stirred for about 24 h. A small quantity of the solution was taken every a stated time, and the concentration of the dye was determined by measuring the absorbance at 200–800 nm using a UV–vis spectrophotometer. Each time before the absorption measurement, the solution and Fe_3O_4/BiOCl catalyst particles was separated by a magnet. Control experiments of direct photolysis and adsorption of dye on the photocatalyst proceeded under the same conditions. The absorption was converted to the dye concentration referring to a standard curve showing a linear behavior between the concentration and the absorption at this wavelength.

2.3.4. Magnetic property measurement

Magnetic measurements carried out using a physical property measurement system (PPMS) at room temperature. The Fe_3O_4/BiOCl powders were taken into a capsule.

3. Results and discussion

3.1. Synthesis and characterization of Fe_3O_4/BiOCl

Chloroform was used as the reagent and oil phase in the synthesis of Fe_3O_4/BiOCl. $Bi(NO_3)_3$ were dissolved in aqueous HNO_3 solution (2 mol/l) then mixed with chloroform solution containing certain amount of SDS and Fe_3O_4 nanoparticles. Ammonia solution was added into the above solution and heated at 80 °C and thus the Fe_3O_4/BiOCl nanocomposite formed. As the surfactant, the SDS molecules played two roles: transferring the hydrophobic ligand-capped Fe_3O_4 nanoparticles from the oil phase to the water phase [21,22]; confining the growth of the BiOCl flakes. For comparison, pure BiOCl flakes were also prepared by the same method except introducing the Fe_3O_4 nanoparticles.

The powder X-ray diffraction (XRD) patterns of the as-synthesized sample and recycled sample were shown in Fig. 1a and b, respectively. It revealed the tetragonal primitive crystal structure which is identical to that of BiOCl (JCPDS 06-0249, space

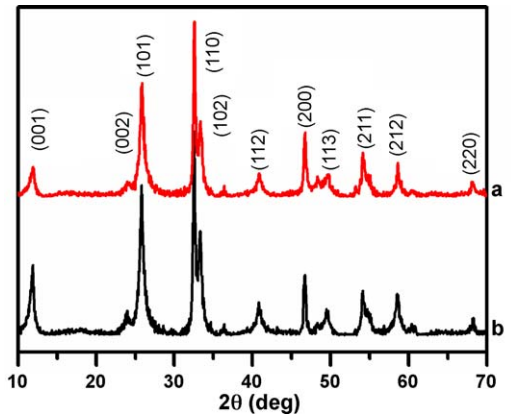

Fig. 1. XRD patterns of (a) Fe_3O_4/BiOCl nanocomposite and (b) recycled Fe_3O_4/BiOCl sample after photocatalysis experiments.

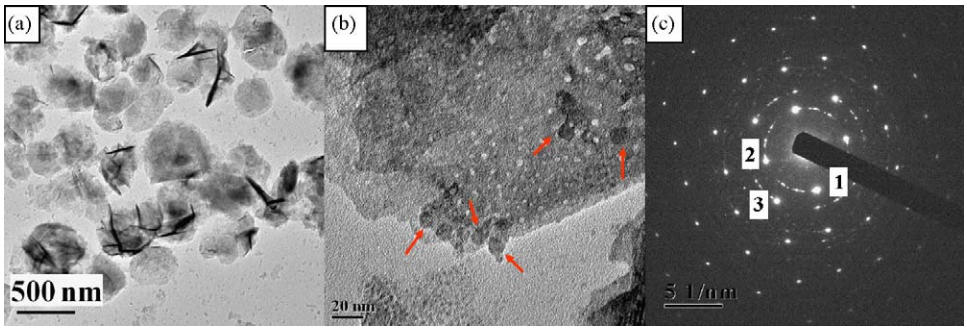

Fig. 2. (a) TEM image of Fe_3O_4/BiOCl nanocomposites flakes; (b) the close-up view of the nanoflake. The arrows directs the Fe_3O_4 nanoparticles; (c) SAED image of (a): spots 1 and 2 were reflected from (2 2 0) of cubic Fe_3O_4 and (1 1 0) of tetragonal BiOCl, spot 3 were reflected from (4 0 0) of cubic Fe_3O_4 and (2 0 0) of tetragonal BiOCl.

group $p4/nmn$, $a = b = 3.891$ Å, $c = 7.369$ Å). The characteristic peaks of Fe_3O_4 were not detected because of its low content (<7%) and weak peaks of nanocrystals. Fig. 2a and b shows the Fe_3O_4/BiOCl nanocomposite comprised of aggregated Fe_3O_4 nanoparticles (7–10 nm) on the large BiOCl flakes. The selected area electron diffraction pattern (SAED, Fig. 2c) shows that the diffraction rings from the (2 2 0) and (4 0 0) Bragg reflections of cubic Fe_3O_4 nanoparticles, and the diffraction spots from the (1 1 0) and (2 0 0) Bragg reflections of the tetragonal BiOCl flake lapped over together due to the coincidence of lattice spacing of the two crystals (see more information in Table S1). It indicates that the lattice cell of BiOCl could coherently grow on the facets of Fe_3O_4 nanocrystals though a straightforward epitaxial growth relationship is missing. The phenomenon was also found in most of the analyzed heterostructures [23–26]. Furthermore, analysis of the high-resolution TEM (HRTEM, Fig. 3a and b) images shows the clear lattice spacing of the flake matrix is about 2.75 Å, which is consistent with the *d*-spacing (2.75 Å) of the [1 1 0] reflection of BiOCl. The lattice fringes of Fe_3O_4 nanocrystals are also found in the same image by using fast Fourier transform (FFT) and the mask method (as shown in Fig. 3c). It shows the Fe_3O_4 nanocrystals are inlaid in the BiOCl flakes matrix but not simply "laid" on the BiOCl flakes.

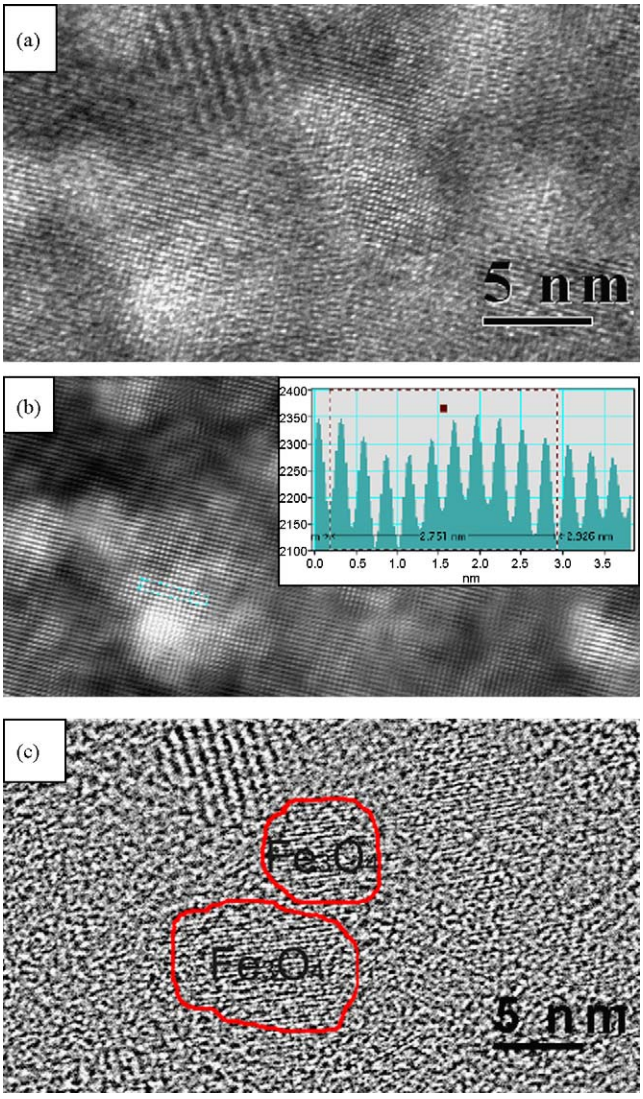

Fig. 3. (a) HRTEM image of Fe_3O_4/BiOCl; (b and c) are obtained by FFT (fast Fourier transform) on (a), and smoothing edge by a mask then inverse FFT, respectively. Inset of (b) exhibits fringes with lattice spacing of ca. 2.75 Å, which correspond to the (1 1 0) plane of tetragonal BiOCl. It approves the matrix flake of the as-synthesized composite was BiOCl crystal; the size of the red circles including crystal lattice in (c) was about 7–10 nm. It shows the Fe_3O_4 nanocrystals are inlaid in the BiOCl matrix flake. (For interpretation of the references to color in this figure legend, the reader is referred to the web version of the article.)

3.2. Photocatalytic activity of Fe_3O_4/BiOCl

The photocatalytic activities of the Fe_3O_4/BiOCl was evaluated by the degradation of rhodamine B (RhB) dye in water (30 mg/l) under visible light ($\lambda > 420$ nm) irradiation. It was compared to that of the pure BiOCl flakes. In addition, to distinguish the direct photolysis and the adsorption of RhB dyes on the nanocomposite,

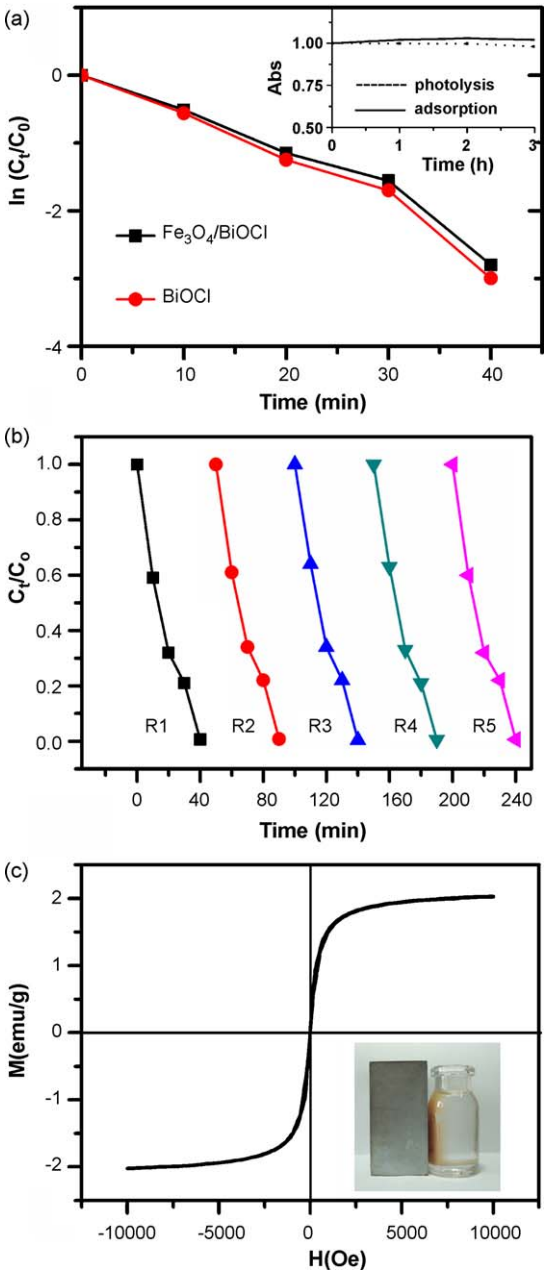

Fig. 4. (a) First-order plots for the photocatalytic degradation of RhB under visible light irradiation using different samples. Inset: absorption changes of directly photolysis and adsorption control experiments; (b) recycle experiments of degrading RhB (30 mg/l) on the Fe_3O_4/BiOCl under visible irradiation; (c) field-dependent magnetization of Fe_3O_4/BiOCl at 300 K. Inset: a photograph showing magnetic recycle of the Fe_3O_4/BiOCl magnetic photocatalyst.

control experiments proceeded under the same conditions. Fig. 4a represents the variation of $\ln(C_t/C_0)$ with irradiation time over different catalysts under visible light irradiation. The first-order linear relationship was revealed by the plots of the $\ln(C_t/C_0)$ vs. irradiation time. The linear fit reaction rate constant k of the degradation of RhB on BiOCl, Fe_3O_4/BiOCl was −0.071 and −0.066, respectively. The direct photolysis and adsorption of RhB on the Fe_3O_4/BiOCl were neglectable as shown in the inset of Fig. 4a. This result not only reveals RhB was photocatalytically degraded in 40 min under visible light irradiation, but also shows the high photocatalytic activity of BiOCl was kept in the Fe_3O_4/BiOCl though the magnetic component Fe_3O_4 was introduced. Further, other dyes, such as methylene blue, could also be completely degraded by this magnetic photocatalyst (Fig. S1) which proves the capability of as-prepared magnetic photocatalyst Fe_3O_4/BiOCl.

3.3. Stability and recycle of Fe_3O_4/BiOCl

The stability of the photocatalysis of the Fe_3O_4/BiOCl powders was confirmed by repeating the decomposition processes for five times, as shown in Fig. 4b. The recycle experiments show that Fe_3O_4/BiOCl could still decompose the RhB dye completely in the same irradiation time and its intrinsic crystal structure was reserved. Fig. 4c shows the field-dependent magnetism of the recycled Fe_3O_4/BiOCl powders which have no hysteresis at 300 K. It represented that the powders exhibited the superparamagnetic characteristics which is desirable for their applications considering its dispersion and recycle. The inset of Fig. 4c exhibits the magnetic photocatalyst could be conveniently collected from the solution by the magnet.

3.4. Approaching to the mechanism

Comparing with other reported magnetic photocatalysts with core–shell structures, which dramatically lost their intrinsically photocatalytic activity due to the introduction of the magnetic core, the above results have demonstrated the as-synthesized Fe_3O_4/BiOCl reserved as high photocatalytic activity as that of BiOCl. At the same time, it could be easily recycled by the magnet. The reservation of the high efficiency may be originated from two conceivable reasons. Firstly, the Fe_3O_4/BiOCl has a special coupled nanostructure which was different with the core–shell structure: the small Fe_3O_4 nanoparticles implanted on the thin BiOCl flake. Generally, in the TiO_2/iron oxide core–shell structure, the photogenerated electrons in the TiO_2 phase (the band gap value: 3.20 eV) transferred into the lower lying conduction band of Fe_3O_4 (the band gap value: 0.1 eV) and the photogenerated holes transferred to the upper lying valence band of the iron oxide,

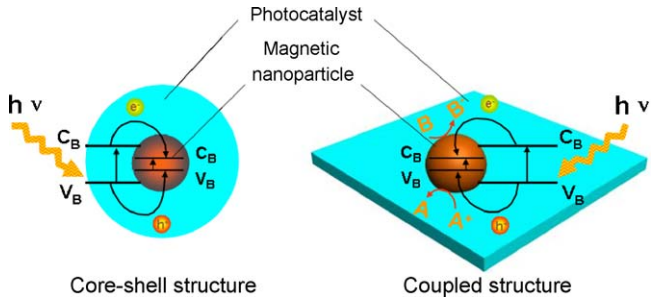

Scheme 1. Scheme of possible charge carrier transfer in magnetic photocatalyst with core–shell structure (left) and as-synthesized Fe_3O_4/BiOCl system (right).

which are difficult to be accessed by any reducing or oxidizing species present in the solution because these carriers would recombine in the Fe_3O_4 core (as shown by the left one in Scheme 1). It may be the main responsible reason for the decrease of the photocatalytic activity. In our study, however, a spot of Fe_3O_4 nanoparticles coupled to the surface of BiOCl flake. Thus, any transferred charge carriers have more opportunities to be accessible for either oxidants or reductants in the solution than that in the core–shell structure, provided that interfacial charge-transfer is faster than the electron–hole recombination (as shown by the right one in Scheme 1). Simulative experiments were also carried out to reinforce this point. The core–shell structure (Fig. 5a) and the coupled structure (Fig. 5b) Fe_3O_4/BiOCl were prepared and corresponding photocatalysis were compared though these samples were larger than the Fe_3O_4/BiOCl discussed in the above. The core–shell structure Fe_3O_4/BiOCl showed weakly photocatalytic activity for degradation organic dye, whereas the coupled structure Fe_3O_4/BiOCl showed effective photocatalytic activity (refer to the detailed information in the supporting information, Fig. S2). Further more, this mechanism has been proved by examining the different charge-transfer between the core–shell structure and the deposition of a semiconductor on the surface of another semiconductor [13,27–29]. Secondly, it is found from the SAED analysis that the similar lattice spacing of the Fe_3O_4 and BiOCl crystals provided the possibility of forming interface with less crystal defects in the Fe_3O_4/BiOCl heterostructure nanocomposite than in the magnetic photocatalyst with other structure. The defects directly increased the recombination opportunity of the electrons and the holes and thus decreased the photocatalytic activities. The similar lattice spacing of these two crystals could reduce the interface energy and be favorable for the growth of BiOCl flake on the Fe_3O_4 seed crystals, because the lowest energy orientation for a phase boundary is the one in which the atom spacing are similar on each side of the boundary [30]. Thus, the

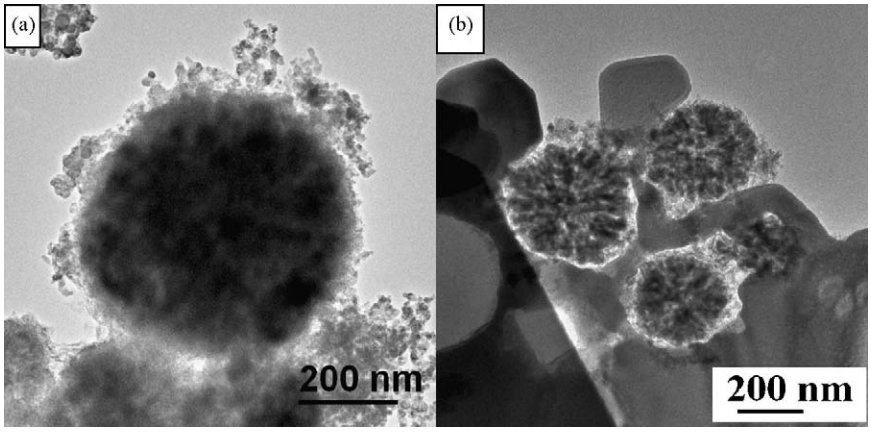

Fig. 5. TEM images of (a) the core–shell structure and (b) the coupled structure of Fe_3O_4/BiOCl.

interface between the Fe_3O_4 and BiOCl crystals did not increase the chances for recombining the electrons and the holes. As a result, the Fe_3O_4/BiOCl showed as high photocatalytic activity as that of the BiOCl flake.

4. Conclusion

In summary, a highly efficient Fe_3O_4/BiOCl magnetic photocatalyst with special coupled nanostructure and interface with fewer defects was realized. It is found that the photocatalytic activities of the Fe_3O_4/BiOCl were kept as that of the BiOCl nanoflakes with layer crystal structure, while the photocatalytic activities of most other magnetic photocatalysts with core–shell structure were dramatically decreased because of the introduction of the magnetic Fe_3O_4 core. The special coupled structure and the interface with fewer defects of the Fe_3O_4/BiOCl are responsible for holding the high photocatalytic activity. These new findings will inspire us to search and design magnetic photocatalysts with new structure and high activity. Moreover, the superparamagnetic Fe_3O_4/BiOCl can be not only easily recycled but also fluidized by applying an external magnetic field. This will enhance both the separation and mixing efficiencies in their further applications in purifying waste water or air.

Acknowledgements

This work was supported by the National Natural Science Foundation of China (No. 50672117), National Basic Research Program of China (973 Program, 2007CB613302) and the Nanotechnology Programs of Science and Technology Commission of Shanghai Municipality (0852nm00500).

Appendix A. Supplementary data

Supplementary data associated with this article can be found, in the online version, at doi:10.1016/j.apcatb.2009.04.005.

References

[1] S. Watson, D. Beydoun, R. Amal, J. Photochem. Photobiol. A 148 (2002) 303–310.
[2] J. Chen, W.H. Rulkens, H. Bruning, Water Sci. Technol. 35 (1997) 231–238.
[3] W.L. Kostedt, J. Drwiega, D.W. Mazyck, S.W. Lee, W. Sigmund, C.Y. Wu, P. Chadik, Environ. Sci. Technol. 39 (2005) 8052–8056.
[4] J. Navio, G. Colon, M. Trillas, J. Peral, X. Domenech, J.J. Testa, J. Padron, D. Rodriguez, M.I. Litter, Appl. Catal. B 16 (1998) 187–196.
[5] K.T. Ranjit, B. Viswanthan, J. Photochem. Photobiol. A 108 (1997) 79–84.
[6] M.I. Litter, J.A. Navio, J. Photochem. Photobiol. A 84 (1994) 183–193.
[7] R.I. Bickley, T. Gonzalez-Carreno, A.R. Gonzalez-Elipe, G. Munuera, L. Palmisano, J. Chem. Soc., Faraday Trans. 90 (1994) 2257–2260.
[8] S. Kurinobua, K. Tsurusakib, Y. Natuic, M. Kimatac, M. Hasegawac, J. Magn. Magn. Mater. 310 (2007) e1025–e1027.
[9] S.H. Xu, W.F. Shangguan, J. Yuan, J.W. Shi, M.X. Chen, Sci. Technol. Adv. Mater. 8 (2007) 40–46.
[10] J. Huang, T. Konishi, T. Shinohara, S. Tsujikawa, Zairyo-to-Kankyo 47 (1998) 193–199.
[11] J. Huang, T. Shinohara, S. Tsujikawa, Zairyo-to-Kankyo 469 (1997) 651–661.
[12] G.H. Li, N.M. Dimitrijevic, L. Chen, J.M. Nichols, T. Rajh, K.A. Gray, J. Am. Chem. Soc. 130 (2008) 5402–5403.
[13] J. Zhang, Q. Xu, Z.C. Feng, C. Li, Angew. Chem., Int. Ed. 47 (2008) 1766–1769.
[14] X. Zong, H. Yan, G. Wu, G. Ma, F. Wen, L. Wang, C. Li, J. Am. Chem. Soc. 130 (2008) 7176–7177.
[15] K.L. Zhang, C.M. Liu, F.Q. Huang, C. Zheng, W.D. Wang, Appl. Catal. B 68 (2006) 125–129.
[16] X.P. Lin, T. Huang, F.Q. Huang, W.D. Wang, J.L. Shi, J. Phys. Chem. B 110 (2006) 24629–24634.
[17] W.D. Wang, F.Q. Huang, X.P. Lin, Scripta Mater. 56 (2007) 669–672.
[18] J. Henle, P. Simon, A. Frenzel, S. Scholz, S. Kaskel, Chem. Mater. 19 (2007) 366–373.
[19] X.Y. Chen, Z.J. Zhang, S.W. Lee, J. Solid State Chem. 181 (2008) 166–174.
[20] X. Zhang, Z.H. Ai, F.L. Jia, L.Z. Zhang, J. Phys. Chem. C 112 (2008) 747–753.
[21] H. Fan, K. Yang, D.M. Boye, T. Sigmon, K.J. Malloy, H. Xu, G.P. Lüpez, C.J. Brinker, Science 304 (2004) 567–571.
[22] J.Y. Kim, J.E. Lee, J.W. Lee, J.H. Yu, B.C. Kim, K.J. An, Y.S. Hwang, C.H. Shin, J.G. Park, J.B. Kim, T.W. Hyeon, J. Am. Chem. Soc. 128 (2006) 688–689.
[23] R. Buonsanti, V. Grillo, E. Carlino, C. Giannini, M.L. Curri, C. Innocenti, C. Sangregorio, K. Achterhold, F.G. Parak, A. Agostiano, P.D. Cozzoli, J. Am. Chem. Soc. 128 (2006) 16953–16970.
[24] H. Zeng, J. Li, Z.L. Wang, J.P. Liu, S.H. Sun, Nano Lett. 4 (2004) 187–190.
[25] H. Kim, M. Achermann, L.P. Balet, J.A. Hollingsworth, V.I. Klimov, J. Am. Chem. Soc. 127 (2005) 544–546.
[26] Z. Ban, Y.A. Barnokov, F. Li, V.O. Golub, C.J. O'Connor, J. Mater. Chem. 15 (2005) 4660–4662.
[27] K.R. Gopidas, M. Bohorquez, P.V. Kamat, J. Phys. Chem. 94 (1995) 6435–6440.
[28] D. Beydoun, R. Amal, G.K.C. Low, S. McEvoy, J. Phys. Chem. B 104 (2000) 4387–4396.
[29] X.P. Lin, J.C. Xing, W.D. Wang, Z.C. Shan, F.F. Xu, F.Q. Huang, J. Phys. Chem. C 111 (2007) 18288–18293.
[30] J.F. Brazdll, L.C. Glaeser, R.K. Grasselli, J. Phys. Chem. 87 (1983) 5485–5491.